CHAPTER

5

Studying neuronal microtubule organization and microtubule-associated proteins using single molecule localization microscopy

Anaël Chazeau, Eugene A. Katrukha, Casper C. Hoogenraad, Lukas C. Kapitein[1]

Cell Biology, Department of Biology, Faculty of Science, Utrecht University, Utrecht, The Netherlands

[1]*Corresponding author: E-mail: l.kapitein@uu.nl*

CHAPTER OUTLINE

Introduction **128**
1. Rationale and Results **130**
2. Material and Methods: Sample Preparation **135**
2.1 Culturing and Transfecting Primary Hippocampal Neurons 135
2.2 ICC: Buffers, Solutions, Equipment 137
2.3 ICC: Protocols 138
3. Material and Methods: Image Acquisition and Analysis **139**
3.1 Imaging: Buffer, Solutions, Equipment 139
3.2 Imaging: Protocols 140
3.3 Analysis and Reconstruction 141
Conclusion and Perspectives **143**
Acknowledgments **144**
References **144**

Abstract

The formation and maintenance of highly polarized neurons critically depends on the proper organization of the microtubule (MT) cytoskeleton. In axons, MTs are uniformly oriented with their plus-end pointing outward whereas in mature dendrites MTs have mixed orientations. MT organization and dynamics can be regulated by MT-associated proteins (MAPs). Plus-end tracking proteins are specialized MAPs that decorate plus-ends of growing MTs and regulate neuronal polarity, neurite extension, and dendritic

Methods in Cell Biology, Volume 131, ISSN 0091-679X, http://dx.doi.org/10.1016/bs.mcb.2015.06.017

spine morphology. Conventional fluorescence microscopy enables observation of specific cellular components through molecule-specific labeling but provides limited resolution (~250 nm). Therefore, electron microscopy has until now provided most of our knowledge about the precise MT organization in neurons. In the past decade, super-resolution fluorescence microscopy techniques have emerged that circumvent the diffraction limit of light and enable high-resolution reconstruction of the MT network combined with selective protein labeling. However, preserving MT ultrastructure, MAP binding, high labeling density, and antibody specificity after fixation protocols is still quite challenging. In this chapter, we provide an optimized protocol for two-color direct stochastic optical reconstruction microscopy imaging of neuronal MTs together with their growing plus-ends to probe MT architecture and polarity.

INTRODUCTION

Neurons are highly polarized cells organized in multiple branched dendrites, a long axon, and a cell body. This morphological organization underlies specific functions for each compartment. Axons generate and propagate action potentials from the cell body to other target cells, whereas dendrites receive those inputs from multiple other axons. The signal transmission from the axon to dendrites occurs via a polarized and asymmetric structure, the synapse. This morphological and functional compartmentalization presents major challenges for sorting and distribution of subcellular components but also for synapse to nucleus communication (Kapitein & Hoogenraad, 2011; Panayotis, Karpova, Kreutz, & Fainzilber, 2015). It is therefore not surprising that impairment in intracellular transport has been linked to neuronal and synaptic malfunctioning and certain neurodegenerative diseases such as Alzheimer's disease, Huntington's disease and Amyotrophic lateral sclerosis (Encalada & Goldstein, 2014; Millecamps & Julien, 2013).

To establish and maintain such a high degree of polarity, cytoskeletal motor proteins transport basic building blocks along polarized cytoskeletal biopolymers, such as actin filaments (F-actin) and microtubules (MTs). MTs serve as tracks for both kinesin and dynein motor proteins, which move in opposite directions toward the plus- and minus-ends of MTs, respectively (Hancock, 2014; Hirokawa, Niwa, & Tanaka, 2010). MTs are hollow tubes with a diameter of 25 nm consisting of 13 protofilaments of alpha- and beta-tubulin heterodimers. They are highly dynamic and continuously switch between phases of growth and shrinkage, a property called dynamic instability. MT organization and dynamics can be regulated by the tubulin GTPase activity, tubulin isoforms, posttranslational modifications (PTMs) of tubulin and by MT-associated proteins (MAPs) (Atherton, Houdusse, & Moores, 2013; Janke & Kneussel, 2010). Plus-end tracking proteins, such as end-binding (EB) proteins, are specialized MAPs that decorate plus-ends of growing MTs (Akhmanova & Steinmetz, 2008). They regulate MT plus-end dynamics, attach and stabilize MTs at the cell cortex, interact with motor proteins, and recruit signaling factors. In contrast to MT plus-ends, MT minus-ends are believed to be much more stable and are targeted by the γ-tubulin ring complex and its interacting partners, as well as by the

calmodulin-regulated spectrin-associated protein (CAMSAP)/Nezha/Patronin family (Baines et al., 2009; Goodwin & Vale, 2010; Kollman, Merdes, Mourey, & Agard, 2011; Yau et al., 2014). While the γ-tubulin ring complex is required for MT nucleation, CAMSAPs proteins regulate MT minus-end growth and stability leading to the formation of CAMSAP-decorated stretches (Hendershott & Vale, 2014; Jiang et al., 2014; Yau et al., 2014).

MTs are present throughout neuron development in the cell body, axons, and dendrites (Conde & Caceres, 2009). Early work, using the hook-decoration method combined with electron microscopy (EM), reveal that in axons MTs are uniformly oriented with their plus-end pointing outward, whereas in mature dendrites MTs have mixed orientations (Baas, Black, & Banker, 1989; Baas, Deitch, Black, & Banker, 1988; Burton, 1988). Remarkably, a proximal axotomy induces a major reorganization of dendritic MTs into a uniform array of plus-end out MTs, leading to a newly formed axon (Gomis-Ruth, Wierenga, & Bradke, 2008; Stone, Nguyen, Tao, Allender, & Rolls, 2010; Takahashi, Yu, Baas, Kawai-Hirai, & Hayashi, 2007). These observations demonstrate the great importance of properly organizing MT orientations in neurons. It is therefore not surprising that plus- and minus-end MT-binding proteins regulate neuronal polarity, axon specification, axonal transport, dendritic branch formation, dendritic spine morphology, and synaptic plasticity (Conde & Caceres, 2009; Gu et al., 2006; Jaworski et al., 2009; Nakata & Hirokawa, 2003; Yau et al., 2014).

To understand how the precise organization of the MT network contributes to neuronal polarity and selective transport, a detailed reconstruction of the spatial distribution of MTs, as well as their lengths and orientations is required for the cell body, dendrites, and axons. Over the past decades, fluorescence microscopy enabled observation of specific cellular components through molecule-specific labeling. However, conventional fluorescence microscopy is limited by the diffraction of light, giving a limited resolution of ∼250 nm in the lateral direction, whereas many subcellular structures are typically below the diffraction limit. For instance, inter-MT spacing in dendrites and axons are thought to be of 60−70 nm and 20−30 nm, respectively (Chen, Kanai, Cowan, & Hirokawa, 1992). During the last decade, different super-resolution fluorescence microscopy techniques have emerged that allow to circumvent the diffraction limit of light (Huang, Bates, & Zhuang, 2009). In structured illumination microscopy (SIM), the spatial resolution is increased by applying a patterned illumination on the sample. Although it has a limited lateral resolution (∼100−150 nm), SIM is well suited for three-dimensional live imaging of multicellular organisms (Schermelleh et al., 2008; Shao, Kner, Rego, & Gustafsson, 2011; York et al., 2012). In Simulated Emission Depletion Microscopy (STED), resolution increase is obtained by shrinking the point spread function (PSF) of a confocal microscope by overlaying the excitation beam by a doughnut-shaped depletion beam that depletes a doughnut around the focus from excited molecules by stimulated emission. STED can reach a resolution of ∼30 nm and deep tissue and in vivo can be performed (Berning, Willig, Steffens, Dibaj, & Hell, 2012; Urban, Willig, Hell, & Nagerl, 2011). However, high-power

laser used for STED induces high photobleaching and requires high labeling density. Reversible saturable optical fluorescence transitions (RESOLFT) microscopy overcome those drawbacks by exploiting reversibly photoswitchable fluorophores (Hofmann, Eggeling, Jakobs, & Hell, 2005; Testa et al., 2012). Single molecule localization microscopy (SMLM) is based on stochastic switch between "on" and "off" states of fluorescent molecules and localization of the clearly resolved individual fluorophores. Among SMLM, photoactivation localization microscopy (PALM) makes use of photo-switchable fluorescent proteins, stochastic optical reconstruction microscopy (STORM) uses the photoswitching of dye pairs or dyes blinking between the fluorescent and dark state (dSTORM, direct STORM), while ground-state depletion and single-molecule return (GSDIM) makes use of dyes switching between the triplet state and the dark state (Betzig et al., 2006; Folling et al., 2008; van de Linde et al., 2011; Rust, Bates, & Zhuang, 2006). So far, SMLM has reached the highest lateral resolution on biological samples (below 10 nm) and has enabled multicolor three-dimensional imaging as well as live single-particle tracking (Bates, Huang, Dempsey, & Zhuang, 2007; Huang, Wang, Bates, & Zhuang, 2008; Manley et al., 2008; Xu, Babcock, & Zhuang, 2012). However, deep tissue and in vivo imaging is still a challenge and high labeling density is required (Dani, Huang, Bergan, Dulac, & Zhuang, 2010; Jones, Shim, He, & Zhuang, 2011).

SMLM has already provided a better understanding into how protein organization and dynamics underlies neuronal signaling. For instance, recent studies describe the nanoscale organization of neurotransmitter receptors, postsynaptic scaffolds, and F-actin in dendritic spines (Chazeau et al., 2014; Dani et al., 2010; MacGillavry, Song, Raghavachari, & Blanpied, 2013; Nair et al., 2013; Tatavarty, Das, & Yu, 2012; Tatavarty, Kim, Rodionov, & Yu, 2009). Another recent breakthrough was the discovery of actin ring-like structures of $\sim$190 nm periodicity throughout the axon (Xu, Zhong, & Zhuang, 2013; Zhong et al., 2014). This periodicity was also found for other axon components such as spectrins, ankyrin-G, and voltage-gated sodium channels, which could therefore influence how action potentials are generated and propagated. Although SMLM has provided new insights into F-actin nanoscale organization in different neuron compartments, much less is known about the neuronal MT organization. Recently, our laboratory uncovered the subcellular localization of the MT minus-end-binding protein CAMSAP2 in hippocampal neurons using two-color dSTORM imaging (Yau et al., 2014). However, preserving MT ultrastructure MAPs binding, high labeling density, and antibody specificity after fixation is still quite challenging. We therefore provide in this chapter an optimized protocol for two-color dSTORM imaging of the dense neuronal MT network, while preserving the labeled plus-ends of growing MTs.

1. RATIONALE AND RESULTS

Most of our knowledge about precise MT organization in neurons is based on early EM experiments. Indeed, EM has been able to determine MT organization, polarity,

and interspacing in axonal and dendritic bundles (Baas et al., 1988; Burton, 1988; Chen et al., 1992; Yu, Ahmad, & Baas, 1994). However, EM experiments are typically based on a small subset of neurons, and it remains very challenging to combine systematic three-dimensional EM reconstructions with selective labeling of proteins. Therefore, super-resolution fluorescence microscopy and in particular SMLM provides an alternative approach by enabling high-resolution reconstruction of MT networks combined with selective protein labeling such as MAPs. As for EM, obtaining high-quality dSTORM images rely on precise fixation protocols in order to preserve ultrastructural details.

Methanol (MeOH) fixation is often used as a fixative for MT immunocytochemistry (ICC) and conventional diffraction-limited microscopy. MeOH induces dehydration of cells and protein precipitation, resulting in protein denaturation. This induces artifacts in the cellular structure affecting the quality of EM (Schnell, Dijk, Sjollema, & Giepmans, 2012) and SMLM images. Paraformaldehyde (PFA) and glutaraldehyde (GA) are cross-linker fixatives. They covalently link protein residues intra- and intermolecularly and provide a better preservation of MT structure. PFA is a small molecule that penetrates quickly into tissue but its chemical reaction with proteins occurs slowly. On the other hand GA is a stronger fixative, with a fast chemical reaction with proteins, but penetrates tissue slowly (Kiernan, 2000). Considering *in vitro* preparations such as cell cultures, tissue penetration is not a major issue and GA should be a faster fixative than PFA. However, ICC can be severely impaired by GA fixation; autofluorescence due to excess aldehyde groups in the cell environment can be a major concern. Therefore, a combination of PFA and GA as a fixative can be used. However, an additional challenge in using PFA/GA is that such fixation often blocks the epitope for specific antibodies, and thereby prevent the selective labeling of specific structures.

In addition, cytoskeletal components such as F-actin and MT are also present in cell in soluble forms. Whereas MeOH fixation will not preserve these soluble fractions, cross-linking by PFA and GA will fix those soluble fractions and increase the fluorescence background of samples. An extraction protocol was established for preserving actin ultrastructure during EM sample preparations and can be performed either before or during fixation (Auinger & Small, 2008; Jones, Korobova, & Svitkina, 2014; Korobova & Svitkina, 2008; Small, Rottner, Hahne, & Anderson, 1999). This extraction step permeabilizes the cell membrane to enable removal of soluble proteins and reduction of the fluorescence background. This protocol was successfully used for dSTORM imaging of F-actin and MTs (Xu et al., 2012, 2013; Yau et al., 2014).

In order to generate high-quality two-color dSTORM images of MTs together with specific MAPs, we are providing, in this chapter, some insights into how different fixatives affect MT integrity, as well as labeling density and specificity. Since MeOH is often used for MT ICC while extraction plus fixation was shown to be the best for ultrastructure of cytoskeleton, we first performed dSTORM imaging of α-tubulin in neurons with those different fixation methods (Figure 1). Although the MT network seem to be preserved in the conventional fluorescence

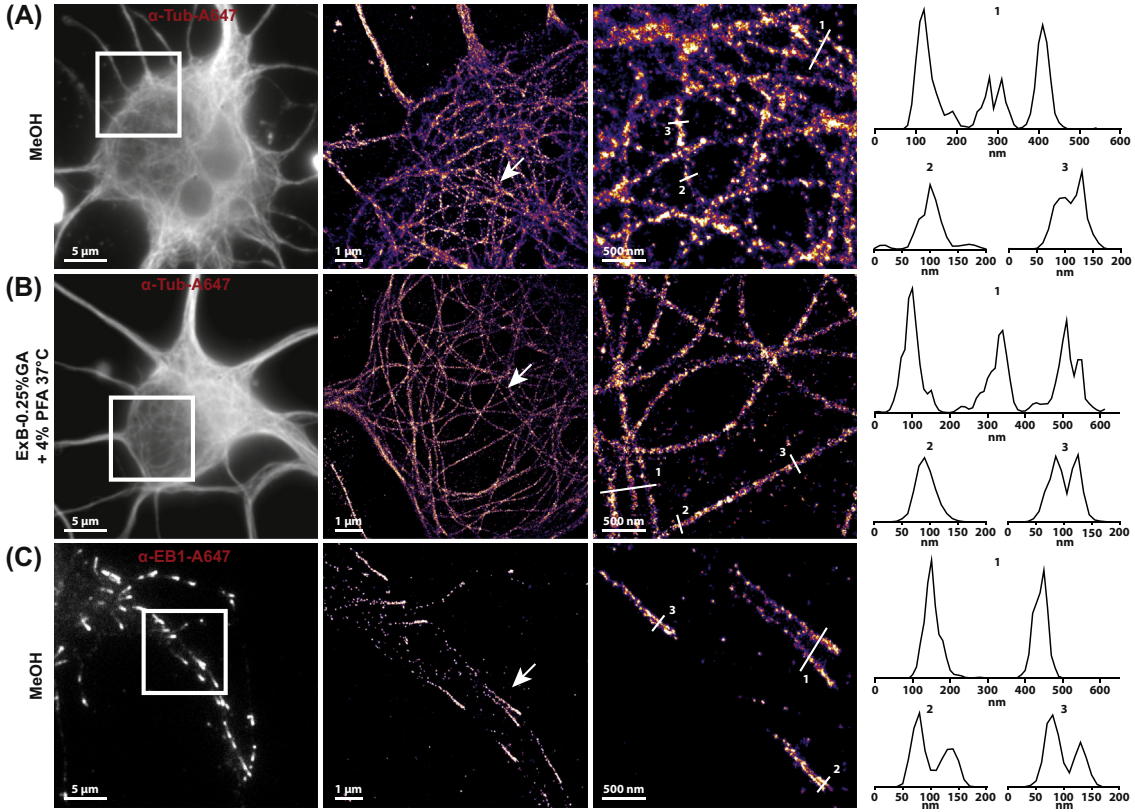

FIGURE 1 Impact of fixatives on SMLM imaging of microtubules (MTs).

(A) DIV 3 neurons fixed with methanol (MeOH) and subsequently fixed with 4% paraformaldehyde (PFA). Neurons were immunostained with primary monoclonal mouse anti-α-tubulin antibody (1:400) and secondary goat anti-mouse A647 (1:400), marked as α-Tub-A647. Left panel: Conventional widefield image. Middle panels: SMLM reconstruction of the box depicted on the left image together with a zoom (pixel size 10 nm). Right panels: linescans (30 nm width) of MTs on the zoom SMLM reconstruction. (B) Same as (A) for a DIV 4 neurons briefly incubated with the extraction buffer containing 0.25% glutaraldehyde (GA) and 0.3% Triton® X100 followed by 4% PFA fixation at 37 °C (ExB-0.25%GA + PFA 4% 37 °C). Note that although individual MTs can be resolved with MeOH fixation, they appear disrupted and discontinuous, unlike MTs in ExB-0.25% GA + PFA 4% 37 °C condition. (C) Same as (A) for a DIV 5 neuron fixed with MeOH and subsequently fixed with 4% PFA, immunostained with primary monoclonal mouse anti-EB1 antibody (1:100) and secondary goat anti-mouse A647 (1:400), marked as α-EB1-A647. (See color plate)

image in MeOH fixed samples, super-resolved images revealed disrupted and discontinuous MTs (Figure 1(A)). Instead, by briefly incubating neurons with our extraction buffer containing 0.25% GA and 0.3% Triton® X100 followed by 4% PFA fixation at 37 °C (ExB-0.25%GA + PFA 4% 37 °C; see Section 2.2 and 2.3), MTs in the super-resolved image appeared as continuous well-defined tubes throughout the neuron (Figure 1(B)). Although MeOH fixation has since been optimized for MTs staining, it still requires a fourfold increase in tubulin antibody concentration and disrupts other cellular structures such as mitochondria and F-actin (Whelan & Bell, 2015).

Since MT growing plus-ends are highly dynamic and unstable, we wondered which fixation method could reliably preserve this structure. To probe growing plus-ends, we imaged EB3-GFP in RPE cells and, for comparison, we tested preservation of more stable MT minus-ends by CAMSAP2-GFP imaging in HeLa cells (Figure 2(A)). Cold MeOH fixation preserved MT plus-ends as well as minus-ends. In contrast, room temperature 4% PFA fixation totally disrupted EB3-GFP localization, while no effect was observed on CAMSAP2-GFP. Switching to 37 °C 4% PFA slightly improved plus-end preservation probably by decreasing MT depolymerization rates (Lodish et al., 2000). Fast and strong fixation with GA enabled preservation of EB3-GFP and CAMSAP2-GFP but significantly increased autofluorescence. Treating the cells with our extraction/fixation protocol (ExB-0.25%GA + PFA 4% 37 °C) greatly reduced autofluorescence background while preserving EB3-GFP and CAMSAP2-GFP integrity, making this protocol comparable with MeOH fixation.

As mentioned above, ICC can be severely impaired by GA. Indeed, whereas protein denaturation in MeOH fixation allowed antibody binding to EB1 and EB3 epitopes and dSTORM imaging (Figures 1(C) and 2(B)), cross-linking by GA totally or partially prevented monoclonal EB1 and polyclonal EB3 antibody binding, respectively (Figure 2(B)). Thus, while the MT network ultrastructure was nicely preserved, endogenous labeling of EBs was prevented. Fortunately, GA fixation did not prevent the recognition of GFP by polyclonal anti-GFP antibodies (Figure 2(B)). Therefore, two-color dSTORM imaging of MTs together with exogenously expressed plus- and minus-end-binding proteins can be reliably performed (Figure 3 and Yau et al., 2014). In order to visualize MT growing plus-ends in neurons, we make use of a GFP-MT+TIP as a general marker to visualize dynamic growing MT plus-ends (Honnappa et al., 2009). By transfecting low concentrations of GFP-MT+TIP in primary hippocampal neurons and making use of our extraction/fixation protocol we can now localize growing MT ends on the dense neuronal MT network (Figure 3).

In the following sections, we will provide our detailed protocol for two-color dSTORM imaging of the neuronal MT network. We will focus on our sample preparation for appropriate MT ICC, while preserving MT ultrastructure and growing plus-ends in primary hippocampal cultured neurons. We will also provide a detailed protocol to collect, analyze and reconstruct two-color dSTORM images.

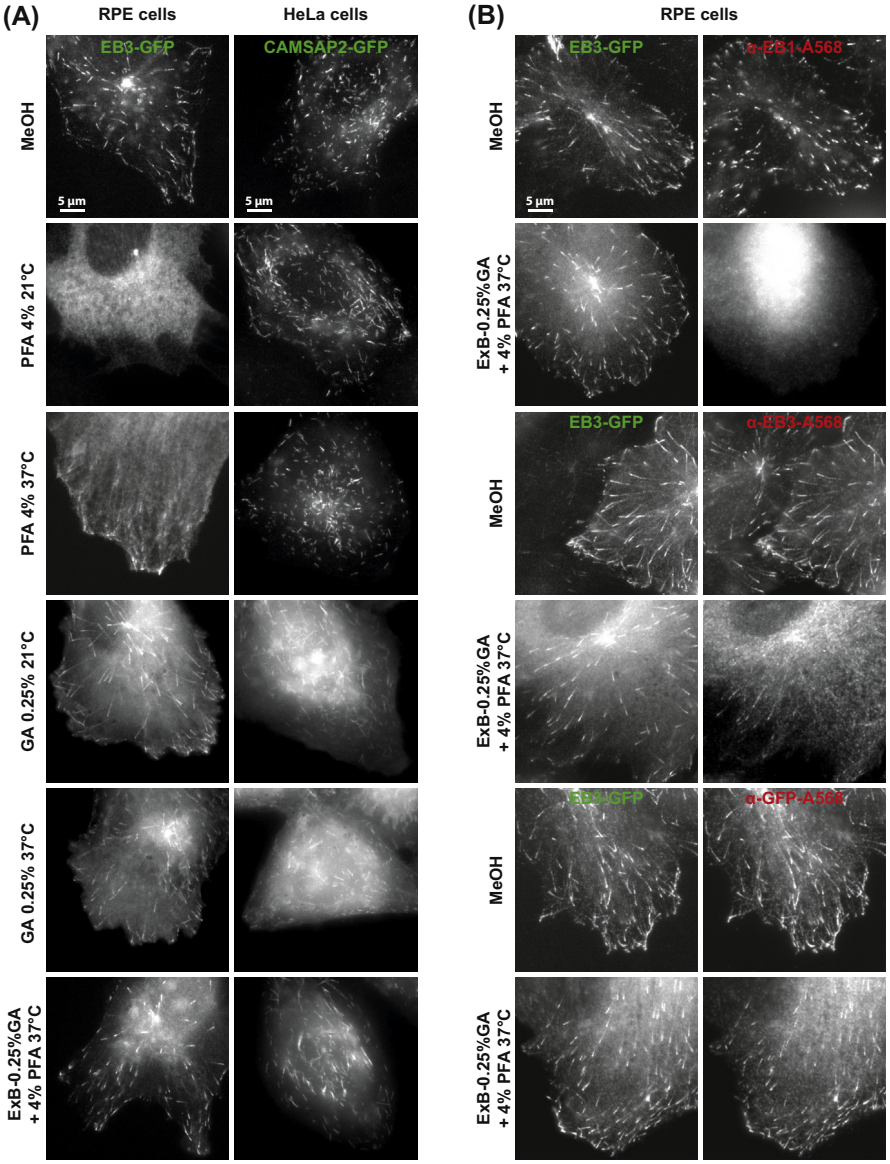

FIGURE 2 Impact of different fixation protocols on MT growing plus-end preservation and antibody specificity.

(A) Left panels: Retinal pigment epithelium (RPE) cells stably expressing EB3-GFP. Right panels: HeLa cells transfected with CAMSAP2-GFP. Cells were fixed with, from top to bottom, methanol (MeOH) (subsequently fixed with 4% paraformaldehyde (PFA)); 4% PFA at room temperature; 4% PFA at 37 °C; 0.25% glutaraldehyde (GA) at room temperature; GA at 37 °C and with extraction buffer containing 0.25% GA and 0.3% Triton® X100 followed by

2. MATERIAL AND METHODS: SAMPLE PREPARATION

2.1 CULTURING AND TRANSFECTING PRIMARY HIPPOCAMPAL NEURONS

Sample preparation is the first step in order to acquire a high-quality STORM image of the neuronal cytoskeleton. Primary hippocampal cultures are prepared from embryonic day 18 (E18) rat brains (Dotti, Sullivan, & Banker, 1988). We previously provided a detailed protocol to culture medium-density primary hippocampal neurons (Kapitein, Yau, & Hoogenraad, 2010). Briefly, neurons are plated on coverslips coated with poly-L-lysine (30 μg/mL) and laminin (2 μg/mL) at a density of 75,000/well. For dSTORM imaging of MTs at latter developmental stages (>DIV7), we recommend a density of 50,000/well. Hippocampal cultures are then grown in Neurobasal medium (NB) supplemented with B27, 0.5 mM glutamine, 12.5 mM glutamate, and penicillin plus streptomycin.

As previously described, hippocampal neurons are transfected using a lipophilic transfection method (Lipofectamine 2000, Invitrogen; Kapitein et al., 2010). For low expression levels of plus-end-binding proteins, we preferentially use a short synapsin promoter (Dittgen et al., 2004). Briefly, we mix 0.1 μg/well of GFP-MT+TIP DNA plus 1.7 μg/well of pGW1 empty vector DNA (12 wells plate) with 3.3 μL of Lipofectamine 2000 in 200 μL of preheated NB, incubate for 30 min, and then add to the neurons in NB at 37 °C in 5% CO_2 for 45–60 min. Neurons are washed with NB and transferred in their original medium at 37 °C in 5% CO_2 and fixed 36–48 h latter.

As an alternative, lentivirus infection can also be performed. It enables a better tuning of transfection efficiency and expression levels, increases transfection efficiency in old neurons, better preserves neuronal health, and it can be used in other preparations such as organotypic hippocampal slices cultures (Schätzle, Kapitein, & Hoogenraad, 2015, in this book).

4% PFA fixation at 37 °C. Note that cold MeOH fixation, but not 4% PFA preserves EB3-GFP localization. GA enables preservation of EB3-GFP, but increases autofluorescence and our extraction/fixation protocol greatly reduces autofluorescence background while preserving EB3-GFP. (B) Left panels: RPE cells stably expressing EB3-GFP, fixed with MeOH (subsequently fixed with 4% PFA) or in the ExB-0.25%GA + PFA 4% 37 °C condition. Right panels: Cells were immunostained with either (top panels) primary monoclonal mouse anti-EB1 antibody (1:100); (middle panels) polyclonal rabbit anti-EB3 antibody (1:300) or (bottom panels) polyclonal anti-GFP antibody (1:500) and subsequently immunostained with secondary goat anti-mouse A568 (1:500) or secondary goat anti-rabbit A568 (1:500). GA totally or partially prevented monoclonal EB1 and polyclonal EB3 antibody binding, respectively, but not polyclonal GFP antibody binding.

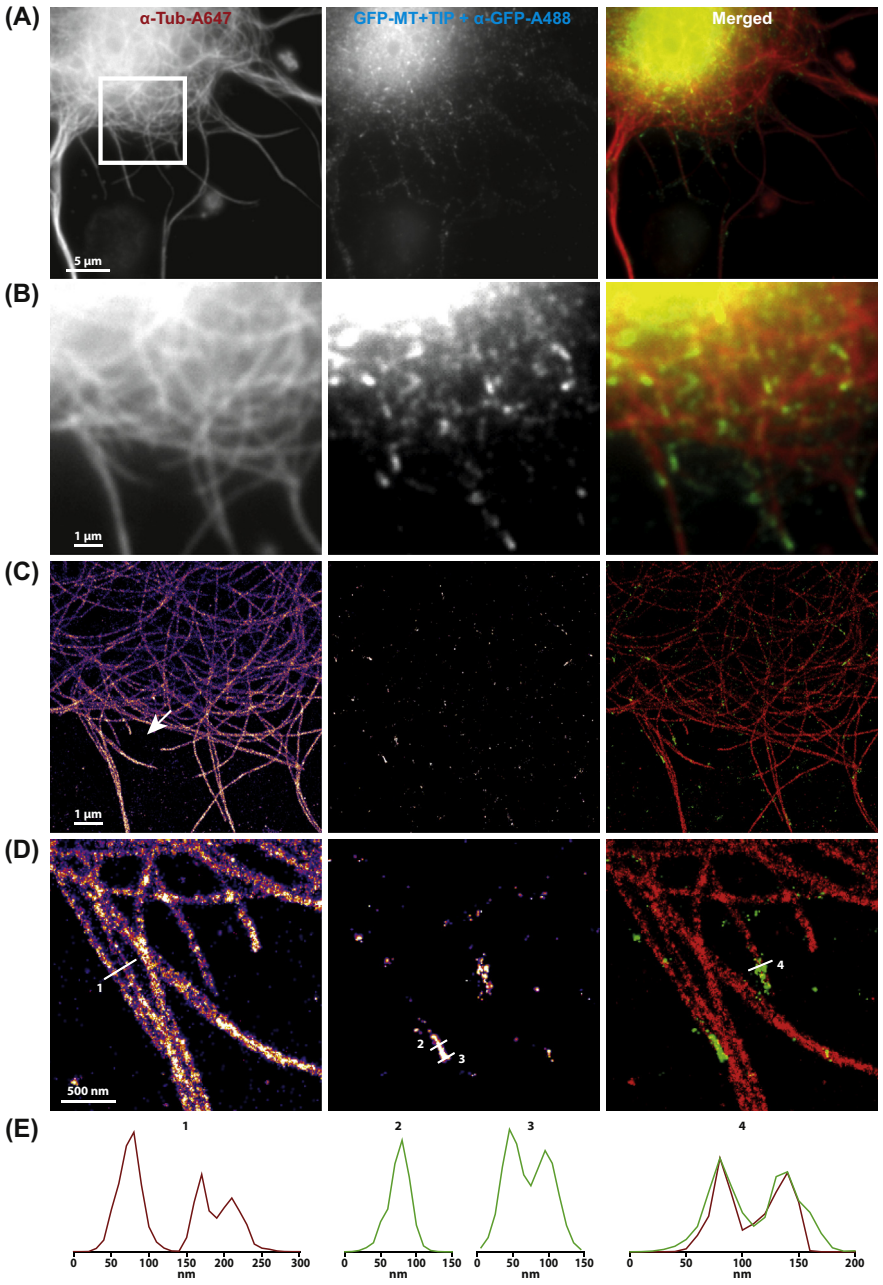

FIGURE 3 Two-color single molecule localization microscopy (SMLM) imaging of MTs with a plus-end-binding protein.

DIV 3 neurons are transfected with GFP-MT+TIP according to the protocol detailed in Section 2.1 and fixed in the ExB-0.25%GA + PFA 4% 37 °C condition. Neurons were

2.2 ICC: BUFFERS, SOLUTIONS, EQUIPMENT

Phosphate-buffered saline (10X PBS from Lonza)
Milli-Q water
MeOH with 1 mM EGTA stored at −20 °C
4% PFA (from Merck) with 4% sucrose (without for nonneuronal cells) stored at −20 °C
2% PFA (from Merck) with 2% sucrose (without for nonneuronal cells) for postfixation.
10% GA (from Electron Microscopy Sciences) stored at 4 °C
Extraction buffer: 80 mM pipes (from Sigma), 7 mM $MgCl_2$, 1 mM EGTA, 0.3% Triton® X100, 150 mM NaCl, 5 mM D-glucose, and 0.25% GA, adjust pH to 6.9 with KOH and keep at 4 °C
10 mM $NaBH_4$ in PBS 1X
Permeabilization buffer: 0.25% Triton® X100 in PBS
Blocking buffer: 2% w/v bovine serum albumine (BSA), 0.2% gelatin, 10 mM glycine, 50 mM NH_4CL in PBS, adjust pH to 7.4 (sterile filtered)
Monoclonal mouse anti-α-tubulin antibody (clone B-5-1-2, Sigma Chemicals)
Monoclonal mouse anti-EB1 antibody (clone 5, BD Bioscience)
Polyclonal rabbit anti-EB3 antibody; produced in-house (Stepanova et al., 2003)
Polyclonal rabbit anti-GFP antibody, (598, MBL)
Alexa Fluor® 647 (A647) goat anti-Mouse IgG (H+L) antibody (A21236, Molecular Probes®, Life Technologies™)
Alexa Fluor® 568 (A568) goat anti-Rabbit IgG (H+L) antibody (A11036, Molecular Probes®, Life Technologies™)
Alexa Fluor® 488 (A488) goat anti-Rabbit IgG (H+L) antibody (A11034, Molecular Probes®, Life Technologies™)
Parafilm® M
Vacuum suction device
Orbital shaker

immunostained with primary monoclonal mouse anti-α-tubulin antibody (1:400) and secondary goat anti-mouse A647 (1:400), marked as α-Tub-A647; and with polyclonal anti-GFP antibody (1:400) and secondary goat anti-rabbit A488 (1:400), marked as GFP-MT+TIP + α-GFP-A488. (A) Conventional widefield image of α-Tub-A647 (left panel) and GFP-MT+TIP + α-GFP-A488 (middle panel) together with the merged image (right panel). (B) Zoom of the depicted box shown in (A). (C) two-color SMLM images of the zoom shown in (B); pixel size 10 nm. (D) Zoom of the depicted region shown in (C); pixel size 10 nm. (E) Linescans (30 nm width) of MTs and GFP-MT+TIP on the zoom SMLM reconstruction. (See color plate)

2.3 ICC: PROTOCOLS

MeOH fixation: Remove the medium from the cells and gently add on the side of the well 1 mL of the MeOH + 1 mM EGTA solution. Incubate cells at −20 °C for 5 min. MeOH is removed, followed by 4% PFA fixation for 5 min at room temperature. To remove leftover fixatives, samples are washed three times for 5 min each with PBS 1X at room temperature on the orbital shaker. This fixation protocol was performed for experiments shown in Figures 1(A, C) and 2(A, B).

PFA fixation: Remove the medium from the cells and gently add on the side of the well 1 mL of 4% PFA for 10 min. For all samples, we recommend to preheat a fresh PFA aliquot to 37 °C and perform the 10 min incubation at 37 °C (Figure 2(A)). To remove the leftover PFA, samples are washed three times for 5 min each with PBS 1X at room temperature on the orbital shaker. This fixation protocol was performed only for experiments shown in Figure 2(A).

GA fixation: Remove the medium from the cells and gently add on the side of the well 1 mL of 0.25% GA (in PBS) for 10 min. To remove the leftover GA, samples are washed three times for 5 min each with PBS 1X at room temperature on the orbital shaker. This fixation protocol was performed only for experiments shown in Figure 2(A). For autofluorescence, no differences were observed between room temperature and 37 °C fixations (Figure 2(A)) but we still recommend performing the 10 min incubation at 37 °C.

Extraction/fixation: Remove the medium from the cells and gently add on the side of the well 1 mL of extraction buffer preheated at 37 °C. Incubate for 90 s in the extraction buffer, remove it and add 1 mL of 4% PFA preheated at 37 °C. This fixation protocol was performed for experiments shown in Figures 1(C), 2(A, B) and 3. To remove the leftover fixatives, samples are washed three times for 5 min each with PBS 1X at room temperature on the orbital shaker. This final washing step was, however, only performed for experiments shown in Figure 2(A) and (B).

Quenching autofluorescence: Autofluorescence due to excess aldehyde groups in the cell environment can be a major concern when preparing dSTORM samples. $NaBH_4$ in PBS 1X reduces free aldehyde groups and can be used to quench autofluorescence. This step is highly recommended when using GA fixation and was performed for experiments shown in Figures 1(C) and 3. During fixation, freshly prepare a solution of 10 mM $NaBH_4$ in PBS 1X. Exchange fixatives with 1 mL of 10 mM $NaBH_4$ in PBS 1X and incubate samples for 7 min. Since $NaBH_4$ can decrease blocking reagents reactivity, quickly wash it one time with PBS 1X followed by two washes of 10 min each with PBS 1X on the orbital shaker.

Permeabilization: Exchange PBS 1X with 1 mL of the permeabilization buffer and incubate for 7 min on the orbital shaker. This allows antibodies to easily enter and access the antigens. This step has been performed in all fixation conditions described above. However, because MeOH also permeabilizes the cellular membrane by dissolving lipids, a permeabilization step can be dispensable. To remove leftover Triton, samples are washed three times for 5 min each with PBS 1X at room temperature on the orbital shaker.

Blocking: Exchange PBS 1X with 1 mL of blocking buffer. The blocking buffer contains reagents that will hinder the antibodies to bind nonspecifically to other proteins. This promotes binding of antibodies to their epitopes.

Indirect ICC: For indirect ICC, we recommend the monoclonal mouse anti-α-tubulin antibody and the rabbit anti-GFP antibody. Dilute the primary antibodies in the blocking buffer to a concentration of 1:400 and drop on a Parafilm® layer 100 μL for each coverslip (18 mm). Transfer the coverslip from the blocking buffer directly onto the drop with cells facing downward. Incubate for 1 h at room temperature. Add fresh PBS 1X to the wells and transfer the coverslips back. To remove unbound antibodies, samples are washed three times for 5 min at room temperature on the orbital shaker. Meanwhile, dilute secondary antibodies in the blocking buffer to a concentration of 1:400 and drop on a Parafilm® layer 100 μL for each coverslip. Transfer the coverslip from the blocking buffer directly onto the drop and incubate for 1 h at room temperature. To protect fluorescently labeled secondary antibodies from light, we recommend performing the antibody incubation in a dark box and covering the sample during all subsequent washes. Add fresh PBS 1X to the wells and transfer the coverslips back. To remove unbound antibodies, samples are washed three times for 5 min at room temperature on the orbital shaker.

Direct ICC: Alternatively to the indirect ICC, one can perform a direct ICC using directly labeled anti-α-tubulin and GFP-targeting nanobodies (Ries, Kaplan, Platonova, Eghlidi, & Ewers, 2012; Yau et al., 2014). We previously provided a detailed protocol for efficient α-tubulin antibody labeling (Cloin, Hoogenraad, Mikhaylova, & Kapitein, 2014). Dilute the primary labeled antibody and nanobody in the blocking buffer to a concentration varying from 1:50 to 1:100 and drop on a Parafilm® layer 100 μL for each coverslip. Transfer the coverslip from the blocking buffer directly onto the drop with cells facing downward. Incubate for 1.5 h at room temperature or overnight at 4 °C. Add fresh PBS 1X to the wells and transfer the coverslips back. To remove unbound antibody/nanobody, samples are washed three times for 5 min at room temperature on the orbital shaker.

PostICC fixation and sample preservation: To decrease antibody dissociation over time, perform a postICC fixation with 2% PFA for 10 min. This will allow cross linking of antibodies to the structure of interest and to each other. To remove the leftover PFA, samples are washed three times for 5 min each with PBS 1X at room temperature on the orbital shaker. Samples can be stored at 4 °C for several days in PBS 1X without any decrease in fluorescence intensity.

3. MATERIAL AND METHODS: IMAGE ACQUISITION AND ANALYSIS

3.1 IMAGING: BUFFER, SOLUTIONS, EQUIPMENT

Microscope slides with single cavity (Globe Scientific)
D-Glucose

β-Mercaptoethylamine (MEA, Sigma Chemicals, 1 M stock stored at −80 °C)
Catalase (Sigma Chemicals)
Glucose oxidase (Sigma Chemicals)
Imaging buffer: 5% w/v D-glucose, 5 mM MEA, 700 μg/mL glucose oxidase, 40 μg/mL catalase in PBS 1X
Vacuum suction device
Multichromatic 100 nm-beads (Tetraspeck™, Invitrogen)
18-mm coverslip, 130−160 nm thick (VWR)
Optical table, vibration isolated (TMC)
Nikon Ti microscope equipped with Perfect Focus System
100x Apo TIRF objective (NA 1.49; oil immersion)
2.5 Optovar to achieve 64 nm pixel size
15 mW 405 nm diode laser (Power Technology)
50 mW 491 nm DPSS laser (Cobolt Calypso)
40 mW 640 nm diode laser (Power Technology)
Andor DU-897D EMCCD camera
Neutral density filters to adjust 405 laser intensity (Thorlabs)
Acousto-optical tunable filter (AOTF, AA Opto Electronic)
Polychroic mirror (zt405/488/561/640rpc, Chroma)
Emission quad-band filter (zet405/488/561/640 nm-EM, Chroma)

3.2 IMAGING: PROTOCOLS

Sample incubation with fiducial markers: As we will describe in the Section 3.3, drift correction can be monitored with the use of multichromatic beads (Tetraspeck™ beads 100 nm). Your coverslip should be incubated with a 1:500 solution of Tetraspeck™ beads in PBS 1X for 15−20 min and quickly washed three times with PBS prior to mounting.

Imaging buffer preparation: For A647 transition into the dark state, fresh MEA is required, we then recommend defreezing an aliquot of 1 mM MEA stored at −80 °C on the day of your experiments. Aliquots of the glucose oxygen scavenging system containing both glucose oxidase and catalase are stored at −80 °C. However, you can keep a working solution at 4 °C for several weeks. Freshly prepare your imaging buffer before mounting each coverslip.

Mounting: To mount the coverslip on the single cavity of the microscopy slide, add 100 μL of imaging buffer to the cavity. Transfer the coverslip onto the cavity with cells facing downward. Press gently on the coverslip and remove excess buffer with the vacuum suction device until the coverslip is securely attach to the slide. The reservoir should be closed in order to reduce influx of oxygen, also make sure they are no air bubbles.

Imaging: Before starting the imaging at the desired position, set TIRF angle, exposure time, and laser power intensities needed for sparse single-molecule density. For A647, the exposure time is set at 20−30 ms and for A488 or Atto488 at 30−40 ms; powers in the order of kW/cm^2 in the sample plane are preferable. If

using Tetraspeck™ beads for drift correction, select an imaging window with at least three beads surrounding the cell. Don't forget to acquire conventional fluorescence images for comparison with super-resolution reconstructions. To prevent bleaching of A647 by illumination with 491 nm laser, start by A647 imaging. Before collecting data, wait until A647 fluorophores switch into the dark state and reach a sparse single-molecule density. Perform a stream acquisition for 5000−20,000 frames. The density of single molecule per frame can be controlled by using 405 nm laser. Sequential A488 streaming acquisition can then be performed. Acquire 5000 and 20,000 frames and also use 405 nm laser to control single-molecule density.

Scanning fiducial markers for chromatic aberration correction: If you previously incubated your sample with Tetraspeck™ beads, you can scan and acquire individual beads from it. If not, at the end of your imaging session, incubate an 18-mm coverslip with a 1:500 solution of Tetraspeck™ beads in PBS 1X for 15−20 min and quickly wash three times with PBS prior to mounting. Multiple images of beads are acquired in both imaging channels. The main aim is to homogeneously cover the whole field of view with approximate density of 2.5−3 beads' images per square micrometer.

3.3 ANALYSIS AND RECONSTRUCTION

Fitting/Reconstruction: The super-resolved image is created by detecting the individual fluorophores and subsequently plotting the probability density of their positions. Coordinates of the fluorophores are determined by fitting of 2D Gaussian function with parameters of microscope's PSF. For our analysis, we use an ImageJ plugin developed in our lab: DoM (https://github.com/ekatrukha/DoM_Utrecht). A variety of alternative detection/fitting methods have been described based on wavelet segmentation and single-particle centroid determination (Izeddin et al., 2012). Several alternative and freely available packages are available such as QuickPALM, RapidSTORM, and μManager (Edelstein, Amodaj, Hoover, Vale, & Stuurman, 2010; Henriques et al., 2010; Wolter et al., 2012).

To detect fluorescent spots corresponding to single molecule, each image in an acquired stack is convoluted with the two-dimensional mexican hat kernel matching the microscope's PSF size. The intensity histogram of the convolved image is fitted to a Gaussian distribution and used to calculate the threshold intensity value (mean value of the fit plus three standard deviations). The maximum intensity values within individual spots are chosen as initial positions for the peaks' fitting performed on the original image. We used the unweighted nonlinear least squares fitting with Levenberg−Marquardt algorithm (Numerical Recipes 3rd Edition: The Art of Scientific Computing, 2007) to the assumed asymmetric two-dimensional Gaussian PSF:

$$I(x,y) = I_{bg} + I_c \exp\left(-\frac{(x-x_c)^2}{2d_x^2} - \frac{(y-y_c)^2}{2d_y^2} \right)$$

where I_{bg}, I_c, x_c, y_c, d_x, d_y are free-fitting parameters. The fit provides coordinates of a molecule x_c and y_c together with localization errors σ_x and σ_y. Only fits with d_x

or d_y values within ±30% of the measured PSF's, standard deviation are accepted. Localizations within one pixel distance in a number of successive frames are considered to arise from the same molecule. In this case, the weighted mean is calculated for each coordinate, where weights are equal to inverse-squared localization errors:

$$\overline{x} = \frac{\sum_i x_i w_i}{\sum_i w_i}, \quad w_i = \frac{1}{\sigma_i^2}, \quad \overline{\sigma}^2 = \frac{1}{\sum_i w_i}$$

where i is an index of successive frame, x_i, σ_i are coordinate and localization error of intensity peak at frame i, and $\overline{x}$, $\overline{\sigma}$ are the final coordinate and the localization error of the molecule. The output of the fitting process is a table containing: fluorophore x- and y-coordinates, errors in their localization, peak and background intensities, and other parameters such as a measure for PSF symmetry.

The resulted table with molecules' coordinates and errors is used to render the final localization image. Each molecule is plotted as a 2D Gaussian of the integrated intensity equal to one and with standard deviations in each dimension equal to the corresponding localization errors. For reconstruction of the super-resolved imaged, two important parameters can be varied: pixel size of the reconstructed image and cutoff value for localization error. According to Nyquist criterion, pixel size should be at least twice as small as the desired resolution. For two-color imaging of MTs together with plus- and minus-end MT-binding proteins, a pixel size between 10 and 20 nm gives optimal quality. Fluorophore localizations with high error can blur the super-resolution reconstruction. In order to improve image quality, the cutoff value for localization error can be used to select only fluorophores with a satisfactory localization precision.

Drift correction: Sample drift is an important issue when considering high localization accuracy. Sample drift during the relatively long imaging time can be caused by thermal changes and mechanical perturbations. Drift can be monitored by the use of fiducial markers adherent to the coverslip whose positions can be tracked in x and y. This approach is ideal for samples with low numbers of localization. However, this approach can be time-consuming when considering the preincubation step of fiducial markers for each coverslip (see Section 3.2) and the probability of finding a transfected neuron with the appropriate number and nicely localized Tetraspeck™ beads. We therefore often use another method for drift correction based on calculating the spatial cross-correlation function between intermediate super-resolved reconstructions (Mlodzianoski et al., 2011). Briefly, the total number of acquired frames is divided in subsets of 500−1000 frames to generate intermediate super-resolved reconstructions. The table of spatial cross-correlation coefficients for various x and y shifts is calculated between each two subsequent intermediate reconstructions and the shift giving the highest correlation coefficient is chosen. The array of shifts in x- and y- coordinates is applied to the each frame of detected results table by linearly approximating its values between consecutive subsets.

Chromatic aberration correction: For two-color imaging, correction of chromatic aberrations induced in the imaging path is performed using TetraSpeck™ beads. Use the stacks obtained by scanning immobilized Tetraspeck™ beads to calculate two consecutive corrections (see Section 2.2). First, a rigid translational correction accounting for the *x* and *y* displacement of one-color channel with respect to another is performed. We are using the maximum projection images of beads in two separate channels and align them using subpixel registration (Guizar-Sicairos, Thurman, & Fienup, 2008). Second, a nonrigid "deformation" within the field of view is performed using Gaussian-fitted positions of beads. We used a point-based registration of 32×32 cells containing a B-spline grid (Rueckert et al., 1999) (http://www.mathworks.com/matlabcentral/fileexchange/20057-b-spline-grid–image-and-point-based-registration), which allows correcting chromatic aberrations with an average error of about 10 nm for the described bead density.

CONCLUSION AND PERSPECTIVES

Super-resolution fluorescence microscopy has become a valuable tool in the field of neurobiology and has already unraveled the nanoscale organization of protein complexes in different neuronal compartments. Here, we have described a simple protocol for high-quality two-color dSTORM imaging of MTs together with their growing plus-ends. We described our sample preparation, image collection procedure, and analysis. We also provide some insights about how different fixatives might affect MT integrity and epitope recognition. Our protocol can also be extended for two-color imaging of MTs together with endogenous labeling of other MAPs and PTMs of tubulin. However, the turnover rate of MAPs on the MT cytoskeleton should be considered when performing an extraction/fixation protocol and antibody binding and specificity should also be tested with different fixatives. To detect PTMs such as polyglutamylation of tubulin, a prefixation with dithiobis succinimidyl propionate was shown to be necessary for midbody MTs (Magiera & Janke, 2013). Finally, other sample preparation protocols have previously been describe for STORM imaging of the cytoskeleton and should be carefully considered, especially when performing two-color imaging together with organelles (Allen, Ross, & Davidson, 2013; Dempsey, 2013; Whelan & Bell, 2015; Xu et al., 2012).

More recently, the development of new molecular tools has started a new era for super-resolution microscopy. First, further development of recombinant antibody-like proteins or CRISPR/Cas9 technology will allow better tagging of endogenous proteins in neurons (Gross et al., 2013; Hsu, Lander, & Zhang, 2014; Incontro, Asensio, Edwards, & Nicoll, 2014). Second, photoswitchable fluorophores are continuously being optimized, enabling, for instance, reliable correlative super-resolution fluorescence microscopy and EM (Paez-Segala et al., 2015; Watanabe et al., 2011). Third, site-specific protein labeling techniques such as Snap-Tag technology was combined with dSTORM imaging to allow live super-resolution microscopy in

three dimensions with a spatial resolution of ~30 nm in the lateral direction and ~50 nm in the axial direction (Jones et al., 2011; Klein et al., 2011). Finally, by linking DNA-PAINT docking strands to antibodies, multiplex SMLM can be achieved (Jungmann et al., 2014, 2010). Further implementation of these techniques should pave the way toward a better understanding of the connection between the MT nanoscale organization and polarized transport in neurons.

ACKNOWLEDGMENTS

We thank Josta Kevenaar, Elena Tortosa, Dieudonné van de Willige and Amélie Fréal for preparing neuronal cultures and Bas Cloin and Marina Mikhaylova for continuous discussions and advice on labeling and imaging conditions. This research is supported by the Netherlands Organisation for Scientific Research NWO (NWO-ALW-VICI to C.C.H and NWO-ALW-VIDI to L.C.K.), the Foundation for Fundamental Research on Matter (FOM), which is part of NWO, and the European Research Council (ERC Consolidator Grant to C.C.H, ERC Starting Grant to L.C.K.).

REFERENCES

Akhmanova, A., & Steinmetz, M. O. (2008). Tracking the ends: a dynamic protein network controls the fate of microtubule tips. *Nature Reviews Molecular Cell Biology, 9*(4), 309–322. http://dx.doi.org/10.1038/nrm2369.

Allen, J. R., Ross, S. T., & Davidson, M. W. (2013). Sample preparation for single molecule localization microscopy. *Physical Chemistry Chemical Physics, 15*(43), 18771–18783. http://dx.doi.org/10.1039/c3cp53719f.

Atherton, J., Houdusse, A., & Moores, C. (2013). MAPping out distribution routes for kinesin couriers. *Biology of the Cell, 105*(10), 465–487. http://dx.doi.org/10.1111/boc.201300012.

Auinger, S., & Small, J. V. (2008). Correlated light and electron microscopy of the cytoskeleton. *Methods in Cell Biology, 88*, 257–272. http://dx.doi.org/10.1016/s0091-679x(08)00414-7.

Baas, P. W., Black, M. M., & Banker, G. A. (1989). Changes in microtubule polarity orientation during the development of hippocampal neurons in culture. *Journal of Cell Biology, 109*(6 Pt 1), 3085–3094.

Baas, P. W., Deitch, J. S., Black, M. M., & Banker, G. A. (1988). Polarity orientation of microtubules in hippocampal neurons: uniformity in the axon and nonuniformity in the dendrite. *Proceedings of the National Academy of Sciences of the United States of America, 85*(21), 8335–8339.

Baines, A. J., Bignone, P. A., King, M. D., Maggs, A. M., Bennett, P. M., Pinder, J. C., et al. (2009). The CKK domain (DUF1781) binds microtubules and defines the CAMSAP/ssp4 family of animal proteins. *Molecular Biology and Evolution, 26*(9), 2005–2014. http://dx.doi.org/10.1093/molbev/msp115.

Bates, M., Huang, B., Dempsey, G. T., & Zhuang, X. (2007). Multicolor super-resolution imaging with photo-switchable fluorescent probes. *Science, 317*(5845), 1749–1753. http://dx.doi.org/10.1126/science.1146598.

Berning, S., Willig, K. I., Steffens, H., Dibaj, P., & Hell, S. W. (2012). Nanoscopy in a living mouse brain. *Science, 335*(6068), 551. http://dx.doi.org/10.1126/science.1215369.

Betzig, E., Patterson, G. H., Sougrat, R., Lindwasser, O. W., Olenych, S., Bonifacino, J. S., et al. (2006). Imaging intracellular fluorescent proteins at nanometer resolution. *Science, 313*(5793), 1642−1645. http://dx.doi.org/10.1126/science.1127344.

Burton, P. R. (1988). Dendrites of mitral cell neurons contain microtubules of opposite polarity. *Brain Research, 473*(1), 107−115.

Chazeau, A., Mehidi, A., Nair, D., Gautier, J. J., Leduc, C., Chamma, I., et al. (2014). Nanoscale segregation of actin nucleation and elongation factors determines dendritic spine protrusion. *EMBO Journal, 33*(23), 2745−2764. http://dx.doi.org/10.15252/embj.201488837.

Chen, J., Kanai, Y., Cowan, N. J., & Hirokawa, N. (1992). Projection domains of MAP2 and tau determine spacings between microtubules in dendrites and axons. *Nature, 360*(6405), 674−677. http://dx.doi.org/10.1038/360674a0.

Cloin, B. M., Hoogenraad, C. C., Mikhaylova, M., & Kapitein, L. C. (2014). Single molecule localization microscopy to study neuronal microtubule organization. *Immunocytochemistry and Related Techniques, Neuromethods, 101*. http://dx.doi.org/10.1007/978-1-4939-2313-7_21.

Conde, C., & Caceres, A. (2009). Microtubule assembly, organization and dynamics in axons and dendrites. *Nature Reviews Neuroscience, 10*(5), 319−332. http://dx.doi.org/10.1038/nrn2631.

Dani, A., Huang, B., Bergan, J., Dulac, C., & Zhuang, X. (2010). Superresolution imaging of chemical synapses in the brain. *Neuron, 68*(5), 843−856. http://dx.doi.org/10.1016/j.neuron.2010.11.021.

Dempsey, G. T. (2013). A user's guide to localization-based super-resolution fluorescence imaging. *Methods in Cell Biology, 114*, 561−592. http://dx.doi.org/10.1016/b978-0-12-407761-4.00024-5.

Dittgen, T., Nimmerjahn, A., Komai, S., Licznerski, P., Waters, J., Margrie, T. W., et al. (2004). Lentivirus-based genetic manipulations of cortical neurons and their optical and electrophysiological monitoring in vivo. *Proceedings of the National Academy of Sciences of the United States of America, 101*(52), 18206−18211. http://dx.doi.org/10.1073/pnas.0407976101.

Dotti, C. G., Sullivan, C. A., & Banker, G. A. (1988). The establishment of polarity by hippocampal neurons in culture. *Journal of Neuroscience, 8*(4), 1454−1468.

Edelstein, A., Amodaj, N., Hoover, K., Vale, R., & Stuurman, N. (2010). Computer control of microscopes using microManager. *Current Protocols in Molecular Biology*, Chapter 14, Unit 14.20. http://dx.doi.org/10.1002/0471142727.mb1420s92.

Encalada, S. E., & Goldstein, L. S. (2014). Biophysical challenges to axonal transport: motor-cargo deficiencies and neurodegeneration. *Annual Review of Biophysics, 43*, 141−169. http://dx.doi.org/10.1146/annurev-biophys-051013-022746.

Folling, J., Bossi, M., Bock, H., Medda, R., Wurm, C. A., Hein, B., et al. (2008). Fluorescence nanoscopy by ground-state depletion and single-molecule return. *Nature Methods, 5*(11), 943−945. http://dx.doi.org/10.1038/nmeth.1257.

Gomis-Ruth, S., Wierenga, C. J., & Bradke, F. (2008). Plasticity of polarization: changing dendrites into axons in neurons integrated in neuronal circuits. *Current Biology, 18*(13), 992−1000. http://dx.doi.org/10.1016/j.cub.2008.06.026.

Goodwin, S. S., & Vale, R. D. (2010). Patronin regulates the microtubule network by protecting microtubule minus ends. *Cell, 143*(2), 263−274. http://dx.doi.org/10.1016/j.cell.2010.09.022.

Gross, G. G., Junge, J. A., Mora, R. J., Kwon, H. B., Olson, C. A., Takahashi, T. T., et al. (2013). Recombinant probes for visualizing endogenous synaptic proteins in living neurons. *Neuron, 78*(6), 971−985. http://dx.doi.org/10.1016/j.neuron.2013.04.017.

Gu, C., Zhou, W., Puthenveedu, M. A., Xu, M., Jan, Y. N., & Jan, L. Y. (2006). The microtubule plus-end tracking protein EB1 is required for Kv1 voltage-gated K+ channel axonal targeting. *Neuron, 52*(5), 803–816. http://dx.doi.org/10.1016/j.neuron.2006.10.022.

Guizar-Sicairos, M., Thurman, S. T., & Fienup, J. R. (2008). Efficient subpixel image registration algorithms. *Optics Letters, 33*, 156–158.

Hancock, W. O. (2014). Bidirectional cargo transport: moving beyond tug of war. *Nature Reviews Molecular Cell Biology, 15*(9), 615–628. http://dx.doi.org/10.1038/nrm3853.

Hendershott, M. C., & Vale, R. D. (2014). Regulation of microtubule minus-end dynamics by CAMSAPs and Patronin. *Proceedings of the National Academy of Sciences of the United States of America, 111*(16), 5860–5865. http://dx.doi.org/10.1073/pnas.1404133111.

Henriques, R., Lelek, M., Fornasiero, E. F., Valtorta, F., Zimmer, C., & Mhlanga, M. M. (2010). QuickPALM: 3D real-time photoactivation nanoscopy image processing in ImageJ. *Nature Methods, 7*(5), 339–340. http://dx.doi.org/10.1038/nmeth0510-339.

Hirokawa, N., Niwa, S., & Tanaka, Y. (2010). Molecular motors in neurons: transport mechanisms and roles in brain function, development, and disease. *Neuron, 68*(4), 610–638. http://dx.doi.org/10.1016/j.neuron.2010.09.039.

Hofmann, M., Eggeling, C., Jakobs, S., & Hell, S. W. (2005). Breaking the diffraction barrier in fluorescence microscopy at low light intensities by using reversibly photoswitchable proteins. *Proceedings of the National Academy of Sciences of the United States of America, 102*(49), 17565–17569. http://dx.doi.org/10.1073/pnas.0506010102.

Honnappa, S., Gouveia, S. M., Weisbrich, A., Damberger, F. F., Bhavesh, N. S., Jawhari, H., et al. (2009). An EB1-binding motif acts as a microtubule tip localization signal. *Cell, 138*(2), 366–376. http://dx.doi.org/10.1016/j.cell.2009.04.065.

Hsu, P. D., Lander, E. S., & Zhang, F. (2014). Development and applications of CRISPR-Cas9 for genome engineering. *Cell, 157*(6), 1262–1278. http://dx.doi.org/10.1016/j.cell.2014.05.010.

Huang, B., Bates, M., & Zhuang, X. (2009). Super-resolution fluorescence microscopy. *Annual Review of Biochemistry, 78*, 993–1016. http://dx.doi.org/10.1146/annurev.biochem.77.061906.092014.

Huang, B., Wang, W., Bates, M., & Zhuang, X. (2008). Three-dimensional super-resolution imaging by stochastic optical reconstruction microscopy. *Science, 319*(5864), 810–813. http://dx.doi.org/10.1126/science.1153529.

Incontro, S., Asensio, C. S., Edwards, R. H., & Nicoll, R. A. (2014). Efficient, complete deletion of synaptic proteins using CRISPR. *Neuron, 83*(5), 1051–1057. http://dx.doi.org/10.1016/j.neuron.2014.07.043.

Izeddin, I., Boulanger, J., Racine, V., Specht, C. G., Kechkar, A., Nair, D., et al. (2012). Wavelet analysis for single molecule localization microscopy. *Optics Express, 20*(3), 2081–2095. http://dx.doi.org/10.1364/oe.20.002081.

Janke, C., & Kneussel, M. (2010). Tubulin post-translational modifications: encoding functions on the neuronal microtubule cytoskeleton. *Trends in Neurosciences, 33*(8), 362–372. http://dx.doi.org/10.1016/j.tins.2010.05.001.

Jaworski, J., Kapitein, L. C., Gouveia, S. M., Dortland, B. R., Wulf, P. S., Grigoriev, I., et al. (2009). Dynamic microtubules regulate dendritic spine morphology and synaptic plasticity. *Neuron, 61*(1), 85–100. http://dx.doi.org/10.1016/j.neuron.2008.11.013.

Jiang, K., Hua, S., Mohan, R., Grigoriev, I., Yau, K. W., Liu, Q., et al. (2014). Microtubule minus-end stabilization by polymerization-driven CAMSAP deposition. *Developmental Cell, 28*(3), 295–309. http://dx.doi.org/10.1016/j.devcel.2014.01.001.

Jones, S. L., Korobova, F., & Svitkina, T. (2014). Axon initial segment cytoskeleton comprises a multiprotein submembranous coat containing sparse actin filaments. *Journal of Cell Biology, 205*(1), 67−81. http://dx.doi.org/10.1083/jcb.201401045.

Jones, S. A., Shim, S. H., He, J., & Zhuang, X. (2011). Fast, three-dimensional super-resolution imaging of live cells. *Nature Methods, 8*(6), 499−508. http://dx.doi.org/10.1038/nmeth.1605.

Jungmann, R., Avendano, M. S., Woehrstein, J. B., Dai, M., Shih, W. M., & Yin, P. (2014). Multiplexed 3D cellular super-resolution imaging with DNA-PAINT and Exchange-PAINT. *Nature Methods, 11*(3), 313−318. http://dx.doi.org/10.1038/nmeth.2835.

Jungmann, R., Steinhauer, C., Scheible, M., Kuzyk, A., Tinnefeld, P., & Simmel, F. C. (2010). Single-molecule kinetics and super-resolution microscopy by fluorescence imaging of transient binding on DNA origami. *Nano Letters, 10*(11), 4756−4761. http://dx.doi.org/10.1021/nl103427w.

Kapitein, L. C., & Hoogenraad, C. C. (2011). Which way to go? Cytoskeletal organization and polarized transport in neurons. *Molecular and Cell Neurosciences, 46*(1), 9−20. http://dx.doi.org/10.1016/j.mcn.2010.08.015.

Kapitein, L. C., Yau, K. W., & Hoogenraad, C. C. (2010). Microtubule dynamics in dendritic spines. *Methods in Cell Biology, 97*, 111−132. http://dx.doi.org/10.1016/s0091-679x(10)97007-6.

Kiernan, J. A. (2000). Formaldehyde, formalin, paraformaldehyde and glutaraldehyde: What they are and what they do. *Microscopy Today, 001*, 8−12.

Klein, T., Loschberger, A., Proppert, S., Wolter, S., van de Linde, S., & Sauer, M. (2011). Live-cell dSTORM with SNAP-tag fusion proteins. *Nature Methods, 8*(1), 7−9. http://dx.doi.org/10.1038/nmeth0111-7b.

Kollman, J. M., Merdes, A., Mourey, L., & Agard, D. A. (2011). Microtubule nucleation by gamma-tubulin complexes. *Nature Reviews Molecular Cell Biology, 12*(11), 709−721. http://dx.doi.org/10.1038/nrm3209.

Korobova, F., & Svitkina, T. (2008). Arp2/3 complex is important for filopodia formation, growth cone motility, and neuritogenesis in neuronal cells. *Molecular Biology of the Cell, 19*(4), 1561−1574. http://dx.doi.org/10.1091/mbc.E07-09-0964.

van de Linde, S., Loschberger, A., Klein, T., Heidbreder, M., Wolter, S., Heilemann, M., et al. (2011). Direct stochastic optical reconstruction microscopy with standard fluorescent probes. *Nature Protocols, 6*(7), 991−1009. http://dx.doi.org/10.1038/nprot.2011.336.

Lodish, H., Berk, A., Zipursky, S. L., Matsudaira, P., Baltimore, D., & Darnell, J. (2000). Microtubule dynamics and associated proteins. In W. H. Freeman (Ed.), *Molecular cell biology* (4th ed., Vol. Section 19.2) New York.

MacGillavry, H. D., Song, Y., Raghavachari, S., & Blanpied, T. A. (2013). Nanoscale scaffolding domains within the postsynaptic density concentrate synaptic AMPA receptors. *Neuron, 78*(4), 615−622. http://dx.doi.org/10.1016/j.neuron.2013.03.009.

Magiera, M. M., & Janke, C. (2013). Investigating tubulin posttranslational modifications with specific antibodies. *Methods in Cell Biology, 115*, 247−267. http://dx.doi.org/10.1016/b978-0-12-407757-7.00016-5.

Manley, S., Gillette, J. M., Patterson, G. H., Shroff, H., Hess, H. F., Betzig, E., et al. (2008). High-density mapping of single-molecule trajectories with photoactivated localization microscopy. *Nature Methods, 5*(2), 155−157. http://dx.doi.org/10.1038/nmeth.1176.

Millecamps, S., & Julien, J. P. (2013). Axonal transport deficits and neurodegenerative diseases. *Nature Reviews Neuroscience, 14*(3), 161−176. http://dx.doi.org/10.1038/nrn3380.

Mlodzianoski, M. J., Schreiner, J. M., Callahan, S. P., Smolkova, K., Dlaskova, A., Santorova, J., et al. (2011). Sample drift correction in 3D fluorescence photoactivation localization microscopy. *Optics Express, 19*(16), 15009−15019. http://dx.doi.org/10.1364/oe.19.015009.

Nair, D., Hosy, E., Petersen, J. D., Constals, A., Giannone, G., Choquet, D., et al. (2013). Super-resolution imaging reveals that AMPA receptors inside synapses are dynamically organized in nanodomains regulated by PSD95. *Journal of Neuroscience, 33*(32), 13204−13224. http://dx.doi.org/10.1523/jneurosci.2381-12.2013.

Nakata, T., & Hirokawa, N. (2003). Microtubules provide directional cues for polarized axonal transport through interaction with kinesin motor head. *Journal of Cell Biology, 162*(6), 1045−1055. http://dx.doi.org/10.1083/jcb.200302175.

Numerical Recipes 3rd Edition: The Art of Scientific Computing. (2007). Cambridge University Press.

Paez-Segala, M. G., Sun, M. G., Shtengel, G., Viswanathan, S., Baird, M. A., Macklin, J. J., et al. (2015). Fixation-resistant photoactivatable fluorescent proteins for CLEM. *Nature Methods*. http://dx.doi.org/10.1038/nmeth.3225.

Panayotis, N., Karpova, A., Kreutz, M. R., & Fainzilber, M. (2015). Macromolecular transport in synapse to nucleus communication. *Trends in Neurosciences, 38*(2), 108−116. http://dx.doi.org/10.1016/j.tins.2014.12.001.

Ries, J., Kaplan, C., Platonova, E., Eghlidi, H., & Ewers, H. (2012). A simple, versatile method for GFP-based super-resolution microscopy via nanobodies. *Nature Methods, 9*(6), 582−584. http://dx.doi.org/10.1038/nmeth.1991.

Rueckert, D., Sonoda, L. I., Hayes, C., Hill, D. L., Leach, M. O., & Hawkes, D. J. (1999). Nonrigid registration using free-form deformations: application to breast MR images. *IEEE Transactions on Medical Imaging, 18*(8), 712−721. http://dx.doi.org/10.1109/42.796284.

Rust, M. J., Bates, M., & Zhuang, X. (2006). Sub-diffraction-limit imaging by stochastic optical reconstruction microscopy (STORM). *Nature Methods, 3*(10), 793−795. http://dx.doi.org/10.1038/nmeth929.

Schätzle, P., Kapitein, L. C., & Hoogenraad, C. C. (2015). Live imaging of microtubule dynamics in organotypic hippocampal slice cultures. *Methods in Cell Biology, 131*, 107−123.

Schermelleh, L., Carlton, P. M., Haase, S., Shao, L., Winoto, L., Kner, P., et al. (2008). Subdiffraction multicolor imaging of the nuclear periphery with 3D structured illumination microscopy. *Science, 320*(5881), 1332−1336. http://dx.doi.org/10.1126/science.1156947.

Schnell, U., Dijk, F., Sjollema, K. A., & Giepmans, B. N. (2012). Immunolabeling artifacts and the need for live-cell imaging. *Nature Methods, 9*(2), 152−158. http://dx.doi.org/10.1038/nmeth.1855.

Shao, L., Kner, P., Rego, E. H., & Gustafsson, M. G. (2011). Super-resolution 3D microscopy of live whole cells using structured illumination. *Nature Methods, 8*(12), 1044−1046. http://dx.doi.org/10.1038/nmeth.1734.

Small, J., Rottner, K., Hahne, P., & Anderson, K. I. (1999). Visualising the actin cytoskeleton. *Microscopy Research and Technique, 47*(1), 3−17. http://dx.doi.org/10.1002/(sici)1097-0029(19991001)47:1<3::aid-jemt2>3.0.co;2−2.

Stepanova, T., Slemmer, J., Hoogenraad, C. C., Lansbergen, G., Dortland, B., De Zeeuw, C. I., et al. (2003). Visualization of microtubule growth in cultured neurons via the use of EB3-GFP (end-binding protein 3-green fluorescent protein). *Journal of Neuroscience, 23*(7), 2655−2664.

Stone, M. C., Nguyen, M. M., Tao, J., Allender, D. L., & Rolls, M. M. (2010). Global up-regulation of microtubule dynamics and polarity reversal during regeneration of an axon from a dendrite. *Molecular Biology of the Cell, 21*(5), 767–777. http://dx.doi.org/10.1091/mbc.E09-11-0967.

Takahashi, D., Yu, W., Baas, P. W., Kawai-Hirai, R., & Hayashi, K. (2007). Rearrangement of microtubule polarity orientation during conversion of dendrites to axons in cultured pyramidal neurons. *Cell Motility and the Cytoskeleton, 64*(5), 347–359. http://dx.doi.org/10.1002/cm.20188.

Tatavarty, V., Das, S., & Yu, J. (2012). Polarization of actin cytoskeleton is reduced in dendritic protrusions during early spine development in hippocampal neuron. *Molecular Biology of the Cell, 23*(16), 3167–3177. http://dx.doi.org/10.1091/mbc.E12-02-0165.

Tatavarty, V., Kim, E. J., Rodionov, V., & Yu, J. (2009). Investigating sub-spine actin dynamics in rat hippocampal neurons with super-resolution optical imaging. *PLoS One, 4*(11), e7724. http://dx.doi.org/10.1371/journal.pone.0007724.

Testa, I., Urban, N. T., Jakobs, S., Eggeling, C., Willig, K. I., & Hell, S. W. (2012). Nanoscopy of living brain slices with low light levels. *Neuron, 75*(6), 992–1000. http://dx.doi.org/10.1016/j.neuron.2012.07.028.

Urban, N. T., Willig, K. I., Hell, S. W., & Nagerl, U. V. (2011). STED nanoscopy of actin dynamics in synapses deep inside living brain slices. *Biophysical Journal, 101*(5), 1277–1284. http://dx.doi.org/10.1016/j.bpj.2011.07.027.

Watanabe, S., Punge, A., Hollopeter, G., Willig, K. I., Hobson, R. J., Davis, M. W., et al. (2011). Protein localization in electron micrographs using fluorescence nanoscopy. *Nature Methods, 8*(1), 80–84. http://dx.doi.org/10.1038/nmeth.1537.

Whelan, D. R., & Bell, T. D. (2015). Image artifacts in single molecule localization microscopy: why optimization of sample preparation protocols matters. *Scientific Reports, 5*, 7924. http://dx.doi.org/10.1038/srep07924.

Wolter, S., Loschberger, A., Holm, T., Aufmkolk, S., Dabauvalle, M. C., van de Linde, S., et al. (2012). rapidSTORM: accurate, fast open-source software for localization microscopy. *Nature Methods, 9*(11), 1040–1041. http://dx.doi.org/10.1038/nmeth.2224.

Xu, K., Babcock, H. P., & Zhuang, X. (2012). Dual-objective STORM reveals three-dimensional filament organization in the actin cytoskeleton. *Nature Methods, 9*(2), 185–188. http://dx.doi.org/10.1038/nmeth.1841.

Xu, K., Zhong, G., & Zhuang, X. (2013). Actin, spectrin, and associated proteins form a periodic cytoskeletal structure in axons. *Science, 339*(6118), 452–456. http://dx.doi.org/10.1126/science.1232251.

Yau, K. W., van Beuningen, S. F., Cunha-Ferreira, I., Cloin, B. M., van Battum, E. Y., Will, L., et al. (2014). Microtubule minus-end binding protein CAMSAP2 controls axon specification and dendrite development. *Neuron, 82*(5), 1058–1073. http://dx.doi.org/10.1016/j.neuron.2014.04.019.

York, A. G., Parekh, S. H., Dalle Nogare, D., Fischer, R. S., Temprine, K., Mione, M., et al. (2012). Resolution doubling in live, multicellular organisms via multifocal structured illumination microscopy. *Nature Methods, 9*(7), 749–754. http://dx.doi.org/10.1038/nmeth.2025.

Yu, W., Ahmad, F. J., & Baas, P. W. (1994). Microtubule fragmentation and partitioning in the axon during collateral branch formation. *Journal of Neuroscience, 14*(10), 5872–5884.

Zhong, G., He, J., Zhou, R., Lorenzo, D., Babcock, H. P., Bennett, V., et al. (2014). Developmental mechanism of the periodic membrane skeleton in axons. *Elife, 3*. http://dx.doi.org/10.7554/eLife.04581.